

Cohesive Zone Modeling of Adhesively Bonded Interfaces: The Effect of Adherend Geometry, Element Selection, and Loading Condition

Devon C. Hartlen*, John Montesano, Duane S. Cronin

*Department of Mechanical and Mechatronic Engineering, University of Waterloo,
200 University Ave W, Waterloo, Ontario, Canada, N2L 3G1*

Abstract

Cohesive zone modeling (CZM) is an efficient technique for modeling adhesively bonded interfaces in structure-level simulations. CZM provides a reduction in computational expense compared to using solid elements and provides a more accurate representation of adhesive response, damage, and failure compared to tiebreak contact methods. Despite these benefits, the adoption of CZM is slowed, in part, due to a lack of information and guidelines as to their appropriate use in industrially relevant modeling situations. While many research studies have applied cohesive elements in conjunction with solid elements to model the adherends, most industrial applications such as automotive structures, are commonly modeled with shell elements. Using CZM to join parts meshed with shell elements requires understanding of how forces and moments are transferred from adherend to adhesive, how the bond line should be modeled geometrically, and how adhesive and adherend parts should be connected numerically. While LS-DYNA® contains several cohesive element formulations, including one specifically developed to be compatible with adherends meshed with shells, and a host of connection techniques, there remains a general lack of understanding as to how CZM should be implemented. To guide the use of CZM, a parametric study was undertaken to examine the effect of cohesive element formulation, adherend element selection, bond line geometry, adherend geometry, and the effect of various connection methods on model response. Two exemplar geometries were explored to examine the effect of different loading condition: a double cantilever beam test and a single lap shear test. It was found that changes in element selection and geometry could dramatically affect the stability and accuracy of the responses of a simulation. Based on the results of this study, this paper presents guidelines and recommended practices for applying CZM to adhesive bond lines for a range of possible modeling scenarios.

Introduction & Background

Originally developed by Dugdale [1] and Barenblatt [2] as a way to represent the stresses at the tip of a crack, cohesive zone modeling (CZM) has evolved into an efficient technique for modeling fracture along a predefined path, such as adhesively bonded interfaces. Finite element (FE) solvers such as LS-DYNA implement CZM using specialized elements known as cohesive elements. Unlike traditional elements that operate on stress and strain tensors, cohesive elements use traction and separation vectors, which provide a substantial reduction in computational expense. Additionally, compared to other connection methods such as tied and tie-break contacts, cohesive elements can provide a more realistic representation of interface response by utilizing material models that reflect actual adhesive behavior. Despite these two advantages, the adoption of CZM and cohesive elements in industry has been slow due, in part, to a lack of guidelines as to their use in industry-relevant modeling scenarios.

Cohesive elements were originally developed for use with adherends discretized with solid elements, where each node of the adherend element has three translational degrees of freedom. As a result, classical cohesive element formulations also have three translational degrees of freedom at each node. A classical cohesive element formulation is available in LS-DYNA as the type 19 solid element [3], or as it will be referred to of this paper, the type 19 cohesive element.

In practice, shell elements are more commonly used when modeling of large structures, such as automotive crash simulations. Furthermore, unlike solid elements, the nodes of a shell element have both translational and rotational degrees of freedom which classical cohesive elements (type 19 cohesive elements) cannot reconcile. To remedy this issue, a formulation that converts the rotational degrees of freedom of a shell element into translational loads applied to the cohesive element has been developed (the type 20 solid element in LS-DYNA [3]). Additionally, there are no available guidelines as to the best way to model an adhesive bond line geometrically.

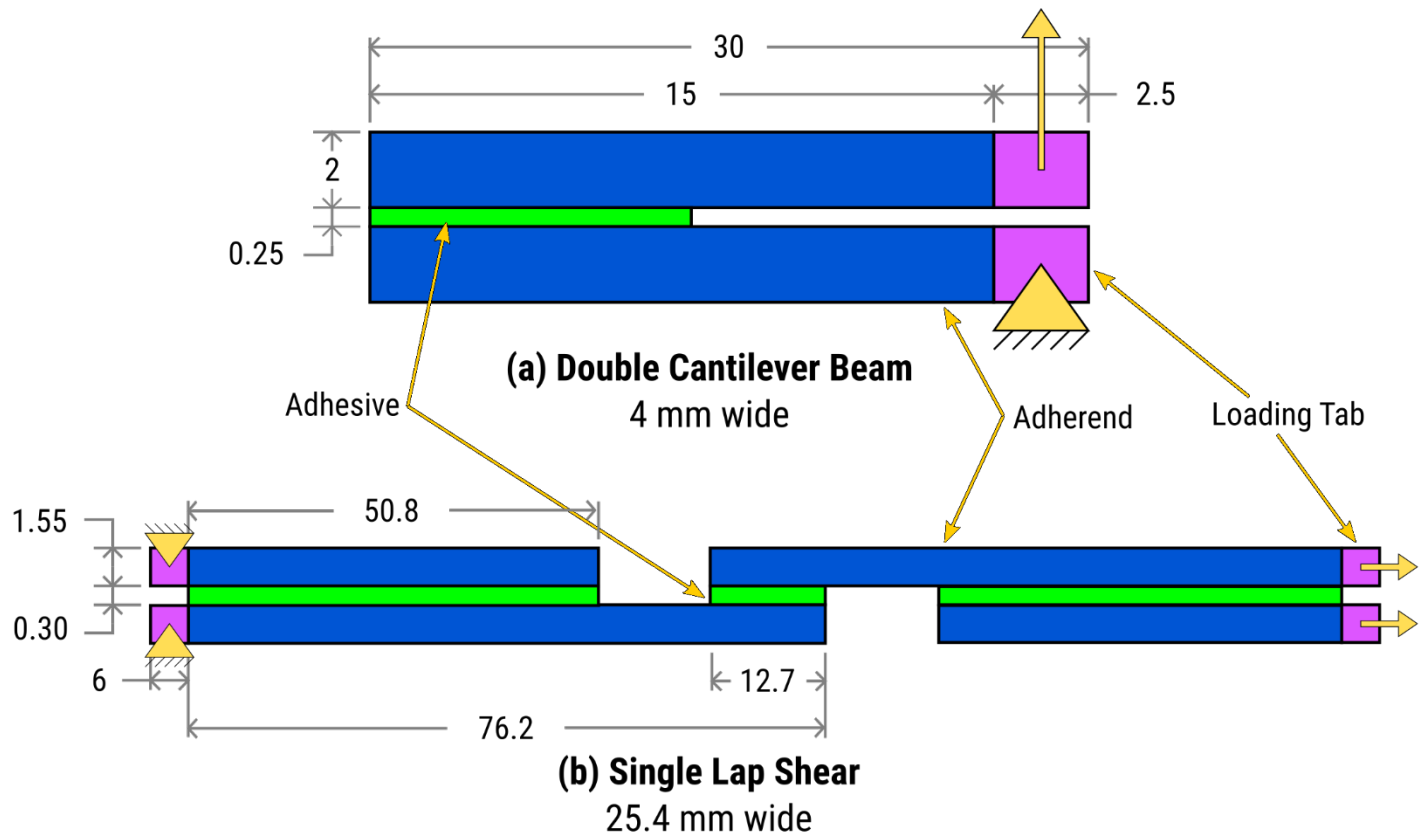


Figure 1: Dimensions of both specimen geometries used in the parametric study. Units are millimeters. Not to scale.

To understand how geometric considerations can change the deformation of the adhesive bond line, a single lap shear joint (Fig 1b) experiencing a pure shear or Mode II loading (Fig. 2a, adhesive in purple) was considered. When the adherend was meshed with solid elements (Fig. 2b), the cohesive elements experienced the same shear deformation as the physical adhesive bond line. However, when the adherend was meshed with shell elements, there were two possible methods to represent the adhesive with cohesive elements. The cohesive elements could span the gap between the midplanes of the shell element adherends (Fig. 2c), acting as a physical connector instead of reflecting actual bond line geometry. While this is somewhat simpler to discretize and visualize, the shear deformation of the cohesive elements was effectively smaller and did not reflect the real geometry of the adhesive, assuming the cohesive element could account for rotational degrees of freedom. An alternative option was to have the cohesive elements reflect the actual bond line geometry (Fig. 2d), respecting the thickness of the shells. While the shear deformation of this option reflected the physical scenario, the connection method used to join adhesive and adherend must faithfully transfer the rotational degrees of freedom of the shells into translational degrees of freedom the cohesive elements can use.

A parametric study was undertaken to understand the effect of discretization strategy, cohesive element formulation, and connection method on overall simulation response. Based on the results of this study, a set of recommendations was developed to help guide the use of cohesive elements when modeling adhesive bond lines and other similar interfaces.

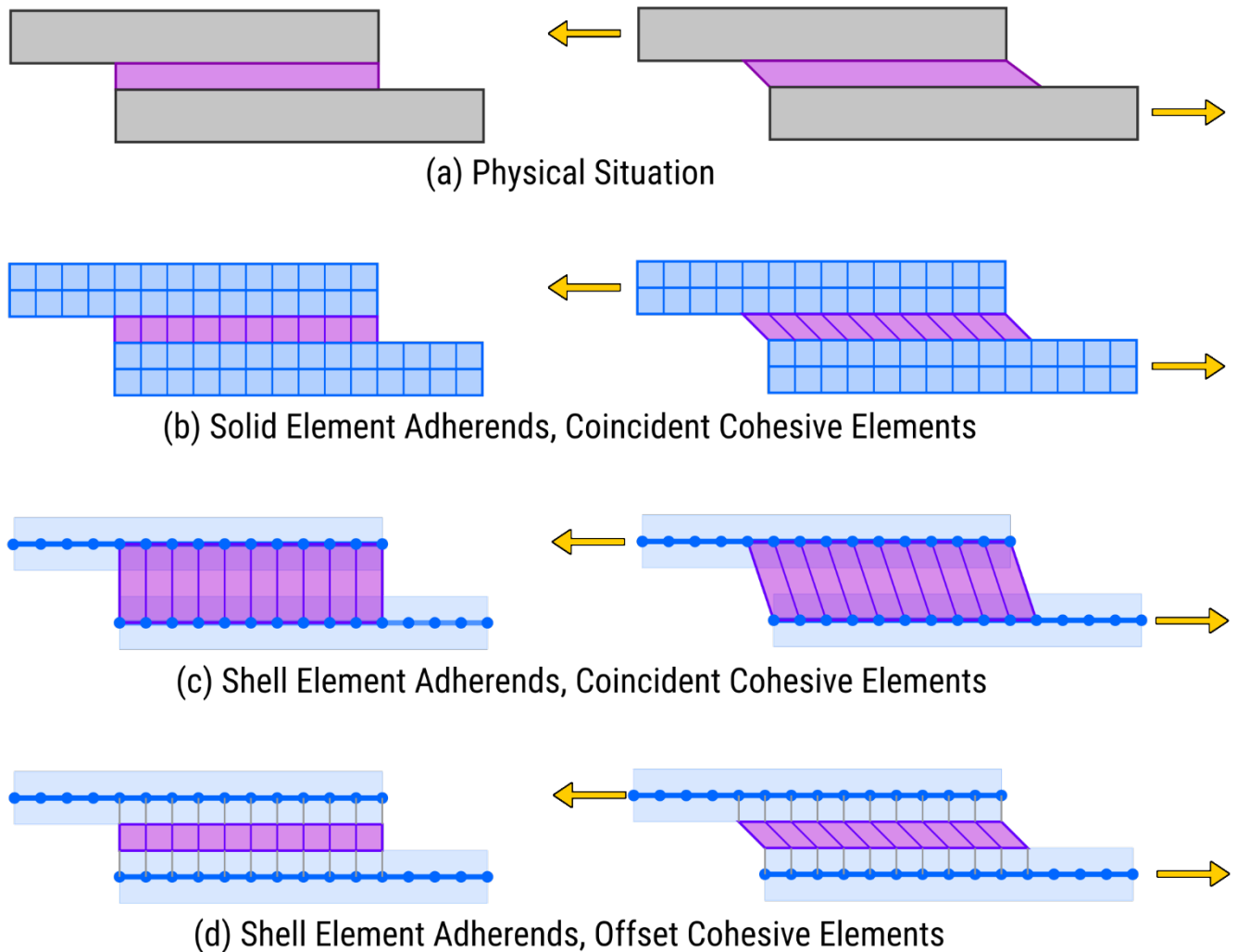


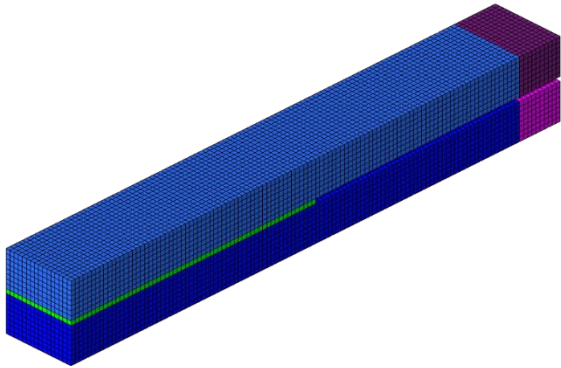
Figure 2: An example of the deformation of an adhesive bondline (purple) undergoing Mode II shear loading. Unloaded geometry is portrayed on the left, while the deformed bondline is shown on the right.

Methods

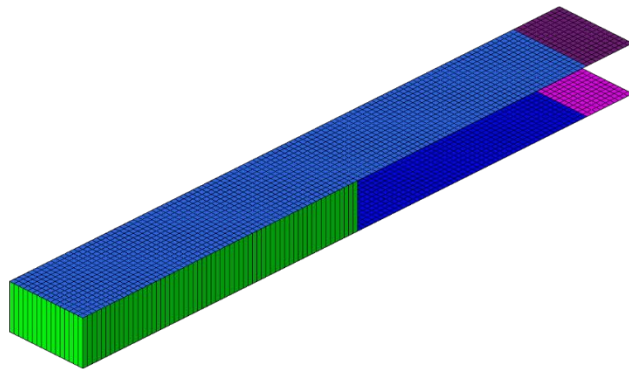
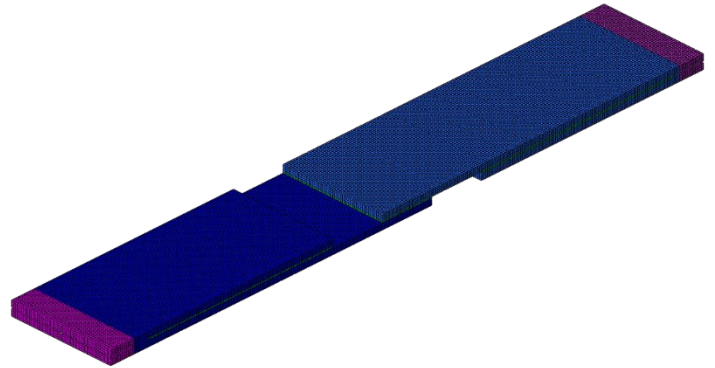
Two exemplar geometries (Fig. 1) were chosen to explore the effect of element type and connection method: a modified version of an adhesive double cantilever beam (DCB) test [4] to explore the effect of pure Mode I loading and a single lap shear (SLS) geometry to understand the effect of Mode II and mixed-mode loading. The SLS geometry used in this work was selected to match the work of Watson *et al.* [5].

Three discretization strategies were investigated for both exemplar geometries (Fig. 3). In the first strategy, the adherends were meshed with solid elements, and the adhesive bond line was modeled geometrically with a single layer of cohesive elements. Type 1 solid elements with type 5 hourglass control were used for the adherends. Two connection techniques to join the cohesive bond line and solid element adherends were examined for this discretization strategy: having the cohesive and solid elements share nodes and connecting adherend and adhesive with `*CONTACT_TIED_NODES_TO_SURFACE`.

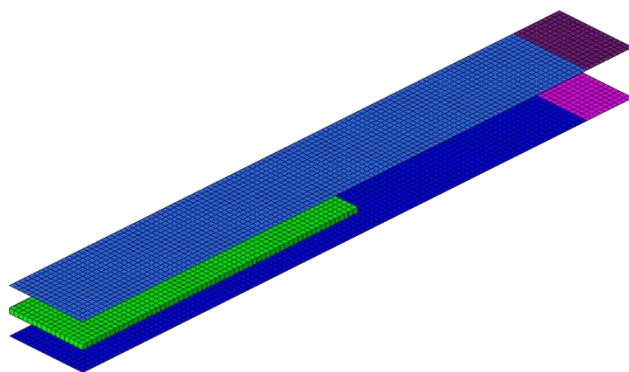
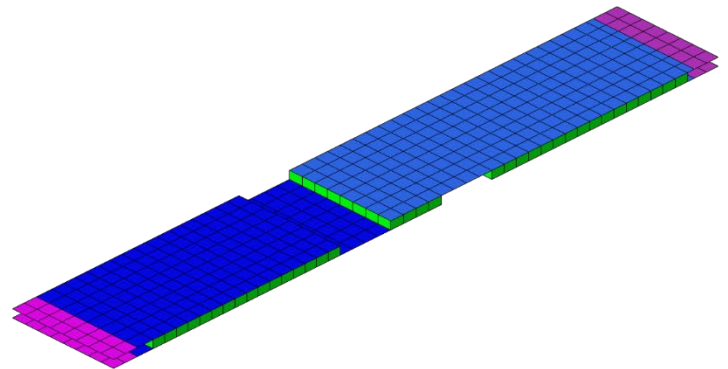
In the second discretization strategy, the adherends were meshed with fully integrated, type 16 shell elements. The adhesive was modeled with a single layer of cohesive elements extending between the midplane of the adherend shells, such that the cohesive elements appear to connect the adherends. As with the first discretization strategy, both shared nodes and tied contact (`*CONTACT_TIED_SHELL_EDGE_TO_SURFACE`) were explored as methods to attach the shell elements of the adherends to the cohesive elements.

Double Cantilever Beam

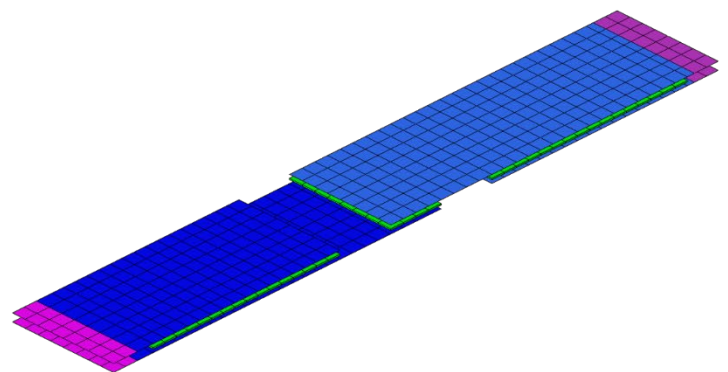
Strategy 1: Solid Element Adherends (Type 1, Hourglass 5), Coincident Cohesive Elements

Single Lap Shear

Strategy 2: Shell Element Adherends (Type 16), Coincident Cohesive Elements



Strategy 3: Shell Element Adherends (Type 16), Offset Cohesive Elements

**Figure 3: The three discretization strategies applied to the two exemplar geometries used in this study.**

In the third strategy, the adherends were once again meshed with type 16 shell elements. However, the adhesive layer was modeled geometrically, such that the thickness of the shells was respected and the cohesive elements represented the physical dimension of the bond line. As the gap between the shell element adherends precludes the use of standard tied contacts, three offset tied contact methods were examined: `*CONTACT_TIED_SHELL_EDGE_TO_SURFACE_BEAM_OFFSET`, `*CONTACT_TIED_SHELL_EDGE_TO_SURFACE_CONSTRAINED_OFFSET`, and `*CONTACT_TIED_SHELL_EDGE_TO_SURFACE_OFFSET`.

For each discretization strategy and connection method, two additional cases were examined where the bond line was modeled with type 19 and type 20 cohesive elements. Overall, this parametric study consisted of 14 combinations of discretization strategy, connection method, and element selection per exemplar geometry for a total of 28 cases in total (Fig. 4). Discretization strategies have been numbered to make referencing specific cases easier in the following discussion.

In all discretization strategies, a consistent mesh size was enforced between the adherend and adhesive to ensure that nodes could be shared in addition to using tied contacts. For the DCB configuration, a mesh size of 0.5 mm was used for all discretization strategies. For the SLS geometry, a 1.0 mm mesh was used for the solid adherend strategy. However, the shell-based strategies (discretization strategies two and three) used a less refined 3.0 mm mesh size. While this reduced the accuracy of the fracture prediction slightly compared to the solid adherend strategy, it was necessary to prevent squat shells (where the length of the shell element approach the thickness of

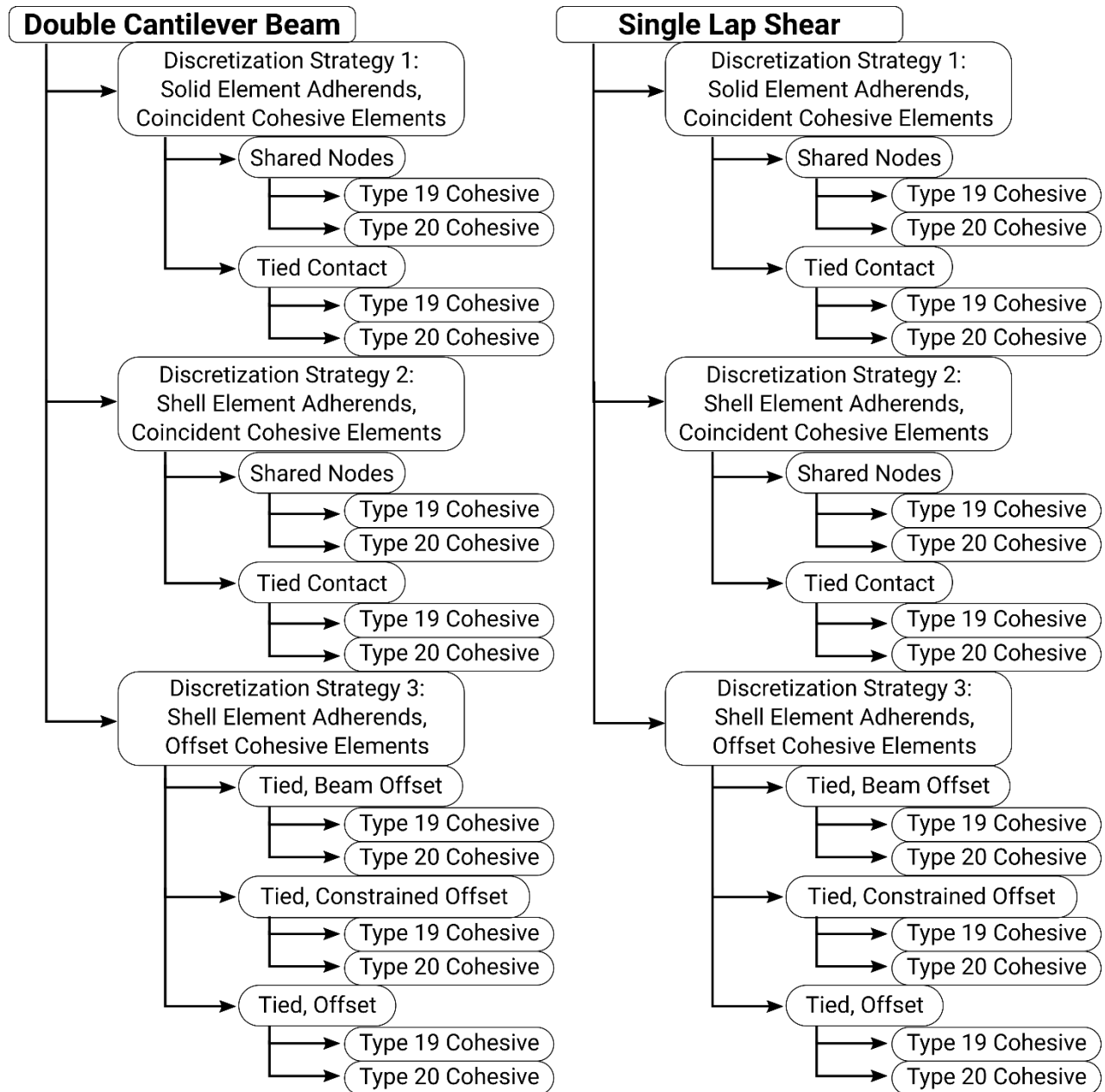


Figure 4: A summary of all cases which were examined in the parametric study.

the shell). For the SLS geometry explored here, the use of shell elements with a length to thickness ratio of less than two resulted in unrealistic behavior as the underlying theory of shell elements was being violated.

The adherends for both geometries were assumed to be elastic and modelled with *MAT_ELASTIC, an assumption valid for adherends made from ultra-high-strength steel [5]. *MAT_COHESIVE_MIXED_MODE_ELASTOPLASTIC_RATE was used to model the adhesive bond line. Constitutive model parameters assigned to the adhesive (Tab. 1) in this work are representative of a commercially available impact-resistant, structural adhesive used in automotive repair. However, they do not match a particular adhesive. The parameter “THICK” was fixed at 1.0 to prevent changes in the physical thickness of the cohesive element between the three discretization strategies from altering constitutive model behavior.

Table 1: Adherend and adhesive constitutive model parameters.

Constitutive Model	Parameters	
*MAT_ELASTIC	$E = 210 \text{ GPa}$ $\rho \text{ (RHO)} = 7850 \text{ kg/m}^3$	$\nu \text{ (NU)} = 0.3$
*MAT_COHESIVE_MIXED_MODE_ELASTOPLASTIC_RATE	$\rho \text{ (RHO)} = 1200 \text{ kg/m}^3$ $K_I \text{ (EMOD)} = 2000 \text{ MPa}$ $G_{IC,0} \text{ (G1C}_0) = 2.00 \text{ N-mm}$ $\sigma_{peak} \text{ (T0)} = 50.0 \text{ MPa}$ $F_{G,I} \text{ (FG1)} = 0.50$	THICK = 1.0 $K_{II} \text{ (GMOD)} = 2000 \text{ MPa}$ $G_{IIC,0} \text{ (G2C}_0) = 8.00 \text{ N-mm}$ $\tau_{peak} \text{ (S0)} = 30.0 \text{ MPa}$ $F_{G,II} \text{ (FG2)} = 0.90$

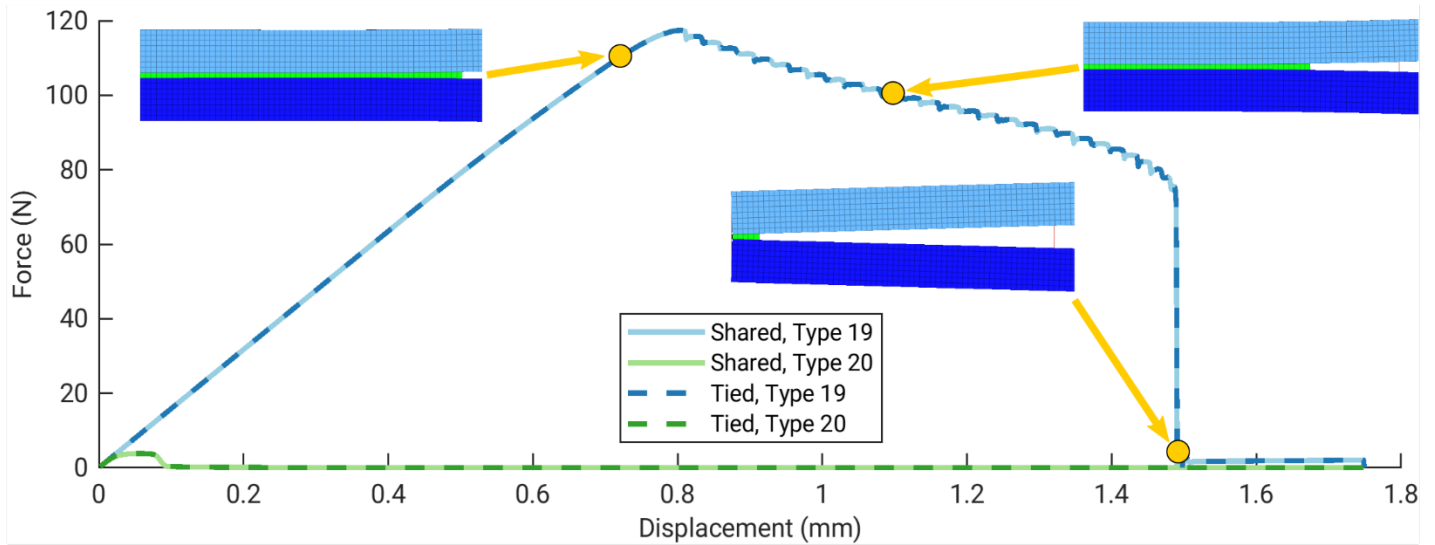
All models were run on a Linux-based compute cluster (CentOS). The same LS-DYNA solver version (R9.2.0 MPP) and the number of cores (32 cores) were used to solve all models to eliminate possible issues of version and core dependence. The effect of discretization strategy, joining technique, and cohesive element selection were benchmarked qualitatively using force-displacement responses and quantitatively using force at yield and work.

Results and Discussion

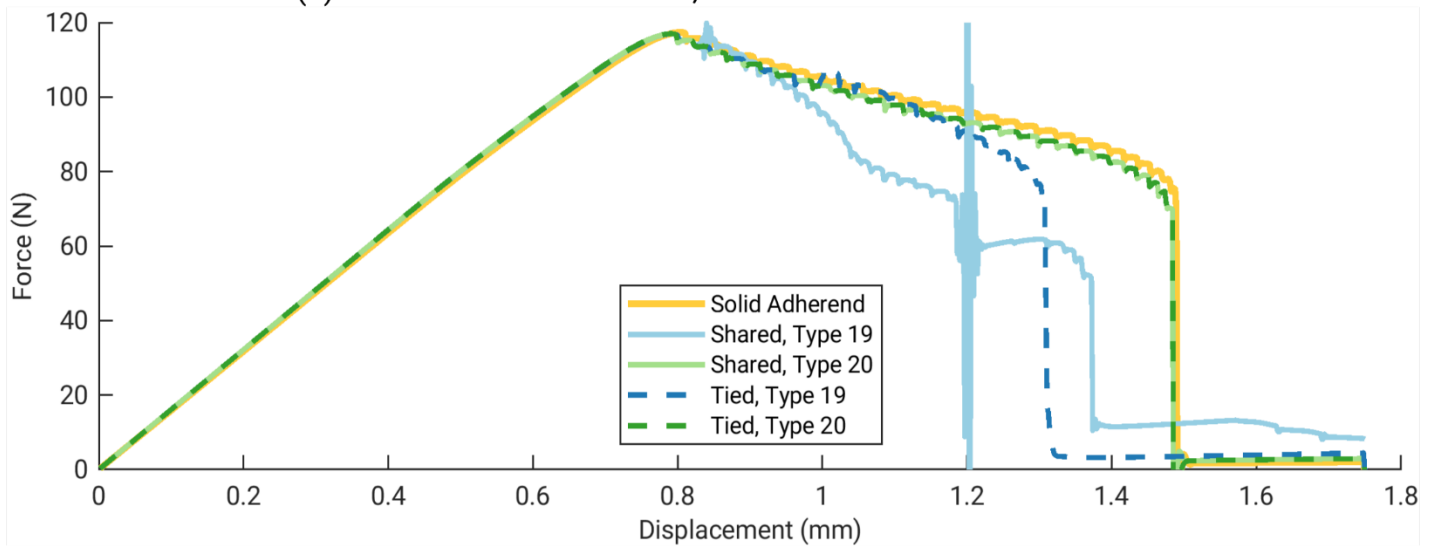
DCB Geometry

Beginning with discretization strategy one (solid element adherends, Fig. 5a), it was apparent that the type 19 cohesive element was preferable over the type 20 cohesive element, which produced non-physical responses. This finding was not unexpected, as the classical cohesive element formulation encompassed by the type 19 cohesive element was designed to work with solid elements. Both force-displacement responses, as well as peak force and work (Tab. 2), showed that both shared nodes and tied contact produced identical results. Fig. 5a shows how the force-displacement response relates to the progressive failure of the adhesive bond line. The force-displacement behavior for discretization strategy one using type 19 cohesive elements and shared nodes was plotted on the remaining subplots to baseline for comparison between discretization strategies.

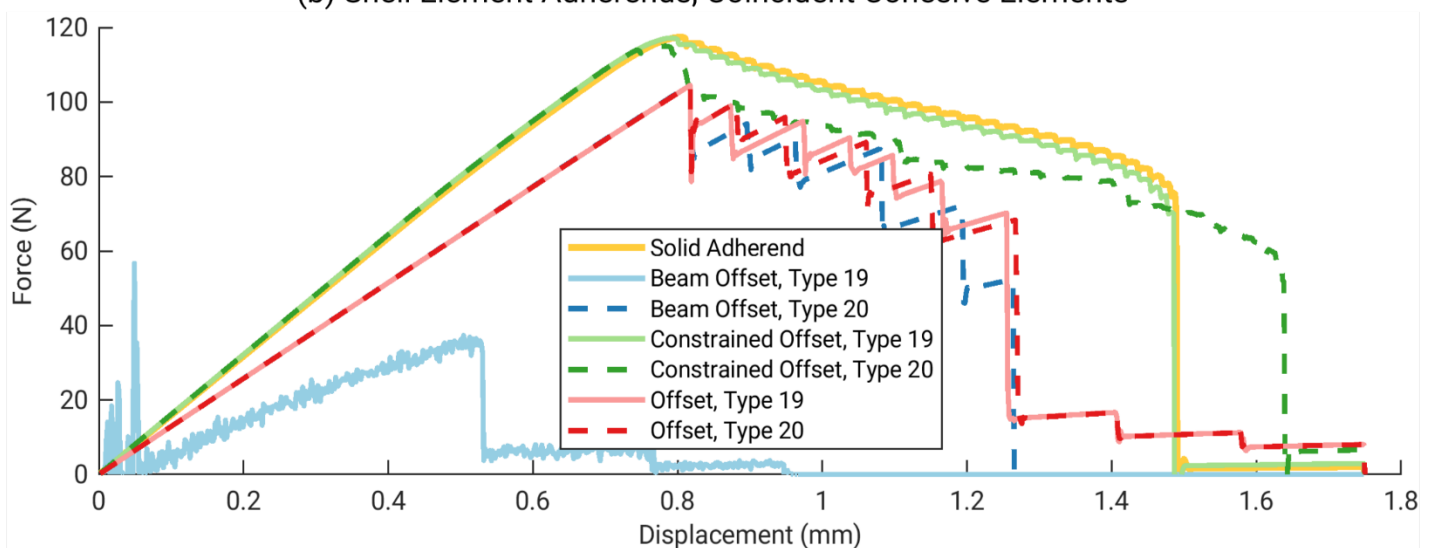
The force-displacement responses of the discretization strategy two DCB models (shell adherends with coincident cohesive elements, Fig. 5b) showed the type 20 cohesive elements was preferable over type 19 for this strategy. Both shared nodes and tied contact produced identical responses, peak forces, and work (Tab. 2) when using the type 20 cohesive element. Note that as the cohesive elements are directly attached to the shell adherends, this would indicate that the type 20 cohesive element was correctly accounting for the rotational degrees of freedom of the shell element adherend. The use of type 19 cohesive elements, which do not account for rotational degrees of freedom, did not produce physically realistic answers. One will also note this discretization strategy agreed well with the first discretization strategy that used solid elements, although small variations are to be expected given the differences in element selection.



(a) Solid Element Adherends, Coincident Cohesive Elements



(b) Shell Element Adherends, Coincident Cohesive Elements



(c) Shell Element Adherends, Offset Cohesive Elements

Figure 5: Force-displacement responses for the DCB geometry for various discretization strategies, cohesive element formulations, and connection methods.

Table 2: Force at yield and work exerted for the DCB geometry.

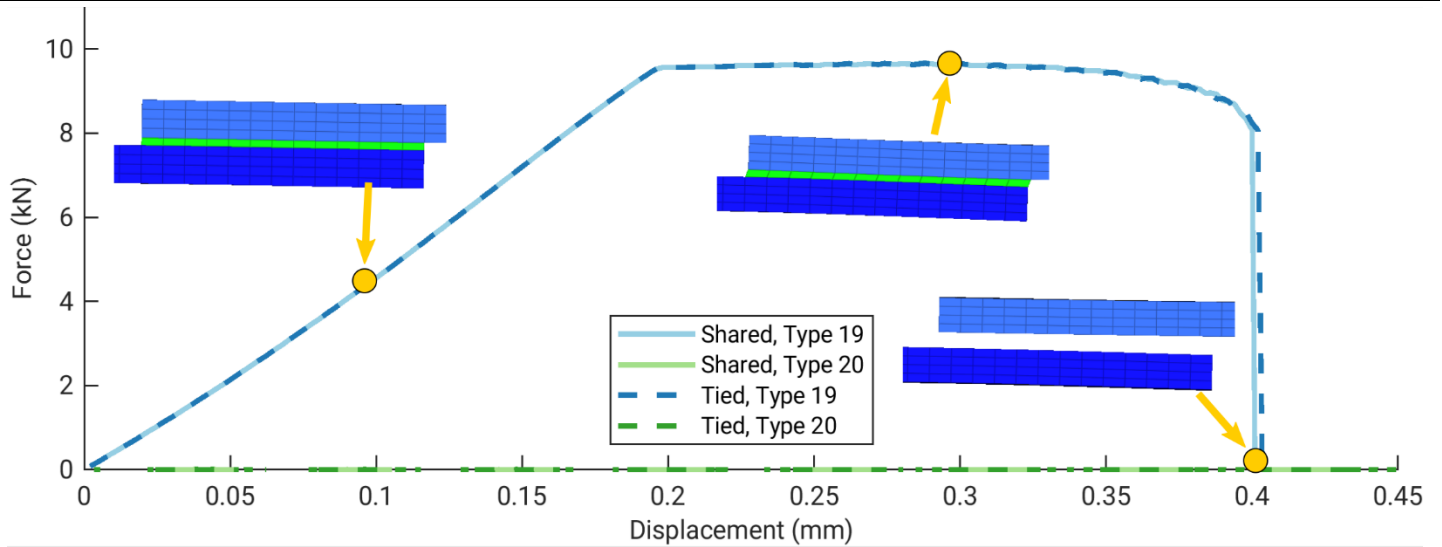
Parametric Study Case	Force at Yield (N)	Work up to 1.75 mm Displacement (mJ)
Strategy 1: Solid Element Adherends, Coincident Cohesive Elements		
Shared Nodes		
Type 19 Cohesive	117.4	118.1
Type 20 Cohesive	3.791	0.3
Tied Contact		
Type 19 Cohesive	117.4	118.1
Type 20 Cohesive	3.791	0.3
Strategy 2: Shell Element Adherends, Coincident Cohesive Elements		
Shared Nodes		
Type 19 Cohesive	117.0	102.6
Type 20 Cohesive	117.0	116.9
Tied Contact		
Type 19 Cohesive	117.0	102.8
Type 20 Cohesive	117.0	116.9
Strategy 3: Shell Element Adherends, Offset Cohesive Elements		
Tied, Beam Offset		
Type 19 Cohesive	36.88	118.9
Type 20 Cohesive	104.6	77.1
Tied, Constrained Offset		
Type 19 Cohesive	117.2	117.2
Type 20 Cohesive	115.0	120.8
Tied, Offset		
Type 19 Cohesive	104.5	84.8
Type 20 Cohesive	104.5	84.9

The force-displacement behavior of the strategy three DCB models (shell adherend with offset cohesive elements, Fig. 5c) showed the selection of offset tied contact method and cohesive element formulation are essential for this discretization strategy. Of all the cases examined for this discretization strategy, only the use of *CONTACT_TIED_..._CONSTRAINED_OFFSET and type 19 cohesive elements produced a force-displacement response which agreed with the previous two discretization strategies.

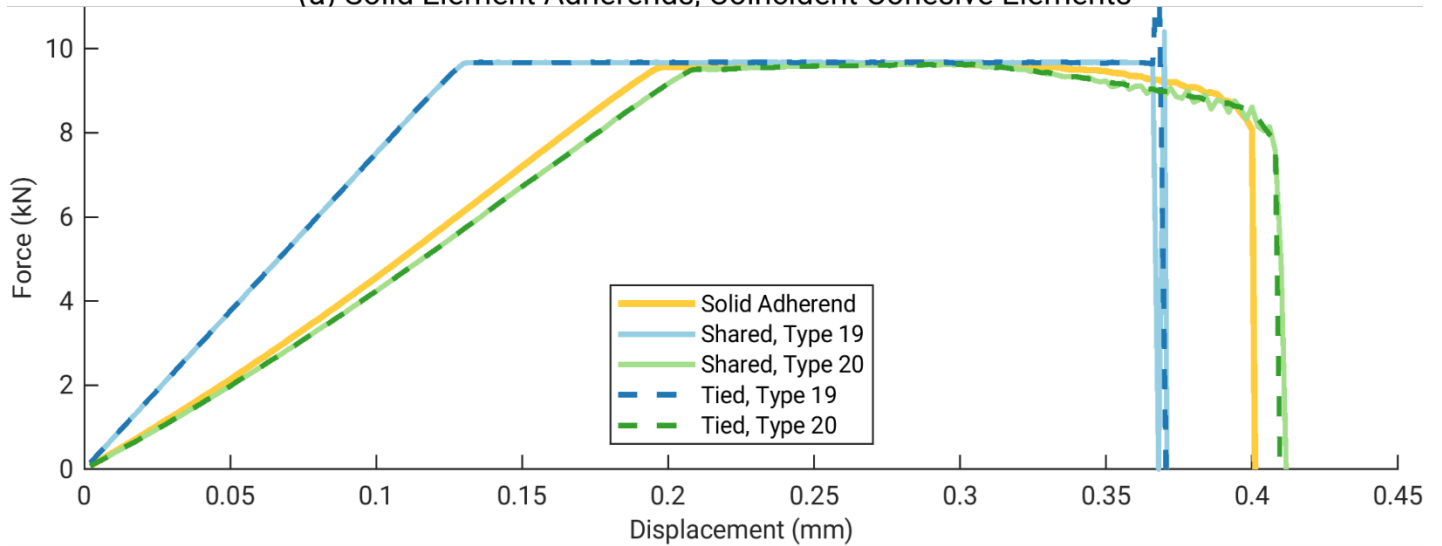
SLS Geometry

Reviewing the response of the discretization strategy one SLS models (solid element adherends, Fig. 6a), only the use of type 19 cohesive elements produced physically realistic responses. The adhesive bondline at various states of loading is also shown in Fig. 6a. Furthermore, these responses agreed in terms of overall shape and magnitude with those reported by Watson *et al.* [5]. This finding is in line with the DCB geometry discussed previously. The force-displacement response of this discretization strategy using shared nodes and type 19 cohesive elements is plotted on the responses of subsequent strategies to provide a baseline.

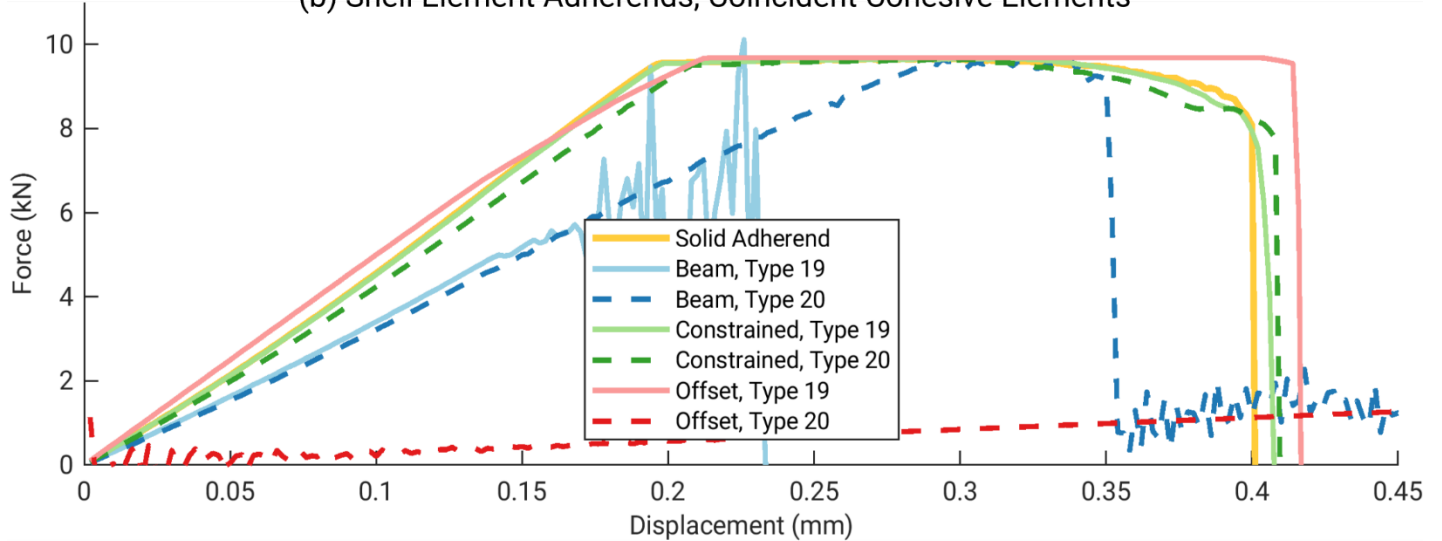
The responses of the discretization strategy two models (shell adherends with coincident cohesive elements, Fig. 6b) make it apparent the use of type 20 cohesive elements, regardless of joining method, provided force-displacement trends, peak forces, and total work that were most similar to the strategy one models. However, unlike the DCB geometry, the use of type 20 cohesive elements with the SLS geometry resulted in reduced initial stiffness compared to the strategy one models, although responses at large deformation did agree well. While force at yield (Tab. 3) is lower than the strategy one models, work was approximately the same. As the initial loading of a single lap shear geometry is predominantly Mode II, the stiffness discrepancy seen here could indicate



(a) Solid Element Adherends, Coincident Cohesive Elements



(b) Shell Element Adherends, Coincident Cohesive Elements



(c) Shell Element Adherends, Offset Cohesive Elements

Figure 6: Force-displacement responses for the SLS geometry for various discretization strategies, cohesive element formulations, and connection methods.

the type 20 cohesive element has a deficiency when handling Mode II loading. While the use of type 19 elements with this discretization strategy produced values of force and work which agreed well with the baseline strategy one SLS models, the force-displacement responses in Fig. 6b exhibited behavior which was markedly different from the baseline model.

Table 3: Force at yield and work exerted for the DCB geometry.

Parametric Study Case	Force at Yield (kN)	Work up to Failure (kJ)
Strategy 1: Solid Element Adherends, Coincident Cohesive Elements		
Shared Nodes		
Type 19 Cohesive	9.559	2.830
Type 20 Cohesive	0.0	0.0
Tied Contact		
Type 19 Cohesive	9.559	2.830
Type 20 Cohesive	0.0	0.0
Strategy 2: Shell Element Adherends, Coincident Cohesive Elements		
Shared Nodes		
Type 19 Cohesive	9.653	2.929
Type 20 Cohesive	9.492	2.823
Tied Contact		
Type 19 Cohesive	9.653	2.925
Type 20 Cohesive	9.492	2.823
Strategy 3: Shell Element Adherends, Offset Cohesive Elements		
Tied, Beam Offset		
Type 19 Cohesive	7.970	0.824
Type 20 Cohesive	9.649	1.986
Tied, Constrained Offset		
Type 19 Cohesive	9.540	2.839
Type 20 Cohesive	9.500	2.804
Tied, Offset		
Type 19 Cohesive	9.661	3.057
Type 20 Cohesive	0.0	0.0

Finally, investigating the force-displacement responses of the third discretization strategy (shell element adherend and offset cohesive element strategy, Fig. 6c), only the use of type 19 cohesive elements with *CONTACT_TIED..._CONSTRAINED_OFFSET resulted in behavior which agrees with all three benchmarks the best. However, unlike the DCB geometry, the use of type 20 cohesively elements and *CONTACT_TIED..._CONSTRAINED_OFFSET also produced responses which only varied from the baseline, strategy one SLS models in initial stiffness and the unrealistic behavior just before adhesive failure. Interestingly, this lower initial stiffness was also seen in the previous discretization strategy when using type 20 cohesive elements.

Based on the results of cases using the type 20 cohesive element in discretization strategies two and three, there is an issue with how the type 20 cohesive element accounts for Mode II loading. In particular, the type 20 cohesive element under-predicts stiffness compared to models using solid adherends or using shell adherends and modeling the bond line geometrically. This behavior does not appear when type 20 cohesive elements are loading in pure Mode I, which may explain why the large deformation behavior of the SLS geometry in Fig. 6b agreed with the strategy one model responses, as the adhesive is experiencing a mixed-mode loading condition at this point.

Conclusions and Recommendations

An investigation of element types, discretization strategies, and connectivity methods was undertaken to determine which options provide the best outcomes when modeling adhesive bond lines with cohesive elements. By means of a parametric study, it was shown that with the correct selection of the aforementioned factors, CZM can present an accurate and efficient alternative to other techniques such as tie-break contacts and traditional solid elements. Based on the findings of this investigation, the following recommendations were developed for implementing cohesive elements:

1. When modeling the adherends with solid elements (discretization strategy one), type 19 cohesive elements are recommended. The cohesive elements can be connected to the solid elements of the adherend using either shared nodes or tied contact.
2. When modeling the adherend with shell elements and the cohesive elements coincident with the midplane of the shell elements (discretization strategy two), type 20 cohesive elements are recommended. These cohesive elements may be connected to the shell elements of the adherend using either shared nodes or tied contact. However, this study has shown that type 20 cohesive elements may underpredict stiffness when placed under Mode II loading.
3. When modeling the adherend with shell elements and offsetting the cohesive elements to account for shell thickness (discretization strategy three), type 19 cohesive elements are recommended. Furthermore, this work has shown that *CONTACT_TIED_..._CONSTRAINED_OFFSET is the only connection method that consistently provides physically realistic responses. Unlike recommendation two, this method is insensitive to loading conditions.

With the appropriate cohesive element formulations and connection methods, FE models applying CZM can effectively model adhesive bond lines and other similar interfaces, regardless of whether the adherends are modeled with shell or solid elements.

References

- [1] D. S. Dugdale, "Yielding of steel sheets containing slits," *J. Mech. Phys. Solids*, vol. 8, no. 2, pp. 100–104, May 1960.
- [2] G. I. Barenblatt, "The Mathematical Theory of Equilibrium Cracks in Brittle Fracture," *Adv. Appl. Mech.*, vol. 7, pp. 55–129, Jan. 1962.
- [3] LSTC, *LS-DYNA Keyword User's Manual Volume I, R9.2.0*. Livermore, USA: LSTC, 2017.
- [4] ASTM International, "D3433-00(2020) Standard Test Method for Fracture Strength in Cleavage of Adhesives in Bonded Metal Joints," West Conshohocken, PA, 2020.
- [5] B. Watson, Y. Nandwani, M. J. Worswick, and D. S. Cronin, "Metallic multi-material adhesive joint testing and modeling for vehicle lightweighting," *Int. J. Adhes. Adhes.*, vol. 95, p. 102421, Dec. 2019